Anal Bioanal Chem (2007) 389:1489–1498
DOI 10.1007/s00216-007-1594-3

ORIGINAL PAPER

Microstructural and chemical transformation of thin Ti/Pd and TiD_y/Pd bilayer films induced by vacuum annealing

W. Lisowski · E. G. Keim · Z. Kaszkur · A. H. J. van den Berg · M. A. Smithers

Received: 7 June 2007 / Revised: 29 August 2007 / Accepted: 31 August 2007 / Published online: 22 September 2007
© Springer-Verlag 2007

Abstract Using a combination of scanning electron microscopy, transmission electron microscopy (TEM), X-ray diffraction and X-ray photoelectron spectroscopy (XPS), we made a comparative study of the high-temperature annealing impact on thin titanium deuteride (TiD_y) films covered by an ultrathin Pd layer, and on Ti/Pd bilayer films. The bilayer films were prepared under ultrahigh vacuum conditions and were in situ annealed using the same annealing procedure. It was found that the surface and the bulk morphology of both films undergo different annealing-induced transformations, leading to an extensive intermixing between the Ti and Pd layers and the formation of a new $PdTi_2$ bimetallic phase. Energy-filtered TEM imaging and energy-dispersive X-ray spectrometry analysis, as well as XPS depth profiling all provided evidence of a different distribution of Pd and Ti in the annealed TiD_y/Pd film compared with the annealed Ti/Pd film. Our results show that thermal decomposition of TiD_y, as a consequence of annealing the TiD_y/Pd film, modifies the intermixing process, thereby promoting Ti diffusion into the Pd-rich top layer of the TiD_y film and thus providing a more likely path for the formation of the $PdTi_2$ phase than in an annealed Ti/Pd film.

Keywords Annealing · Titanium deuteride · Microstructure · X-ray photoelectron spectroscopy

Introduction

Thin Ti/Pd bilayer films can be applied as hydrogen storage material used in catalytic or energetic reactions [1–3]. Thin Ti films are able to form relatively stable titanium hydrides [4–8] and the Pd top layer can protect the titanium hydride material against destructive air interaction [9, 10]. In a previously published paper [10] we presented the results of an extensive structural and chemical characterization of titanium deuteride (TiD_y) films prepared in ultrahigh vacuum (UHV) and in situ covered by a thin evaporated Pd layer (TiD_y/Pd). Evolution of hydrogen from such systems is in practice usually realized at elevated temperatures, where both chemical and structural transformations of the TiD_y/Pd film can be expected to occur as the result of high-temperature annealing and simultaneous decomposition of the TiD_y. With the application of such films as deuterium storage material in mind, a structural and chemical characterization of TiD_y/Pd films after thermal decomposition of the deuteride is highly desirable. Two important questions arise: (1) What will be the tendency of the structural changes of the TiD_y/Pd film towards high-temperature annealing? (2) Would decomposition of deuteride by thermal annealing also affect additionally the structural rearrangement of a Ti/Pd bilayer film? In order to elucidate these points, we performed an experimental investigation using transmission electron microscopy (TEM) in combination with energy-filtered TEM (EF-TEM) and energy-dispersive X-ray spectrometry (EDX), scanning electron microscopy (SEM), X-ray diffraction (XRD) and X-ray photoelectron spectroscopy (XPS). A

W. Lisowski (✉) · Z. Kaszkur
Institute of Physical Chemistry, Polish Academy of Sciences,
Kasprzaka 44/52,
01-224 Warszawa, Poland
e-mail: wlis@ichf.edu.pl

E. G. Keim (✉) · A. H. J. van den Berg · M. A. Smithers
MESA+ Research Institute,
Central Materials Analysis Laboratory, University of Twente,
P.O. Box 217, 7500 AE Enschede, The Netherlands
e-mail: e.g.keim@utwente.nl

comparative study of two types of bilayer films, Ti/Pd and TiD_y/Pd, which underwent a similar annealing procedure, was performed. As we will show, in this way we are able to better characterize the structural variations originating from both high-temperature annealing and deuteride decomposition.

Experimental

Ti films on the order of 100–200-nm thickness were deposited onto a quartz substrate kept at 273 K within a glass UHV system [11], at a pressure of 1×10^{-7} Pa or less, by evaporation of a fine wire (Johnson-Matthey grade I) wound around a tungsten heater. After evaporation, the films were annealed for 60 min at 650 K. The TiD_y films were prepared in situ by volumetrically controlled D_2 sorption on the annealed Ti films at 300 K [12]. Both Ti and TiD_y films were then covered by evaporation of a 10–12-nm-thick Pd layer and were subsequently annealed following the same heating scheme: (1) heating from room temperature to 800 K at a heating rate of 50 K/min, (2) maintaining them at 800 K for 2 h, and (3) cooling from 800 K to room temperature at a rate of 20 K/min. The decomposition of TiD_y as a result of the annealing of the TiD_y/Pd films was also monitored in situ by thermal desorption [13]. The preparation procedure was repeated in situ each time for a new sample. In this way we were able to prepare specimens representative of the Ti/Pd and TiD_y/Pd films prior to annealing and after annealing, respectively.

Morphological examination of all films was performed ex situ in separate analytical systems. TEM analyses were carried out with a Philips CM300ST-FEG instrument which was equipped with a Gatan Tridiem energy filter and a Thermo Fisher Noran System Six EDX analyzer with a nanotrace EDX detector. The TEM specimens of the analyzed films were prepared in cross section according to the recipe described in [14]. Cross-sectional TEM (XS-TEM) as well as energy-filtered TEM (EF-TEM) analyses were used to obtain information regarding the bulk structure of corresponding films, while selected area diffraction (SAD) analysis allowed the crystal phases in the bulk of TiD_y/Pd and Ti/Pd films after annealing to be identified. EDX analysis, used in conjunction with TEM, allows quantification of the relative elemental concentration distributed in selected interface areas of the bilayer films. The surface morphology of all films was revealed using SEM analysis (LEO Gemini 1550 FEG), whereas the crystalline phase characterization of annealed films was realized using XRD (Siemens D 5000 diffractometer).

Additional chemical characterization of the annealed Ti/Pd and TiD_y/Pd films was carried out using XPS (PHI Quantera scanning X-ray microprobe). For calibration of the energy scale of the instrument, the work function of the spectrometer was determined by setting the binding energy (BE) values of Au $4f_{7/2}$, Ag $3d_{5/2}$ and Cu $2p_{3/2}$ for cleaned gold, silver and copper to 83.9, 368.3 and 932.7 eV,

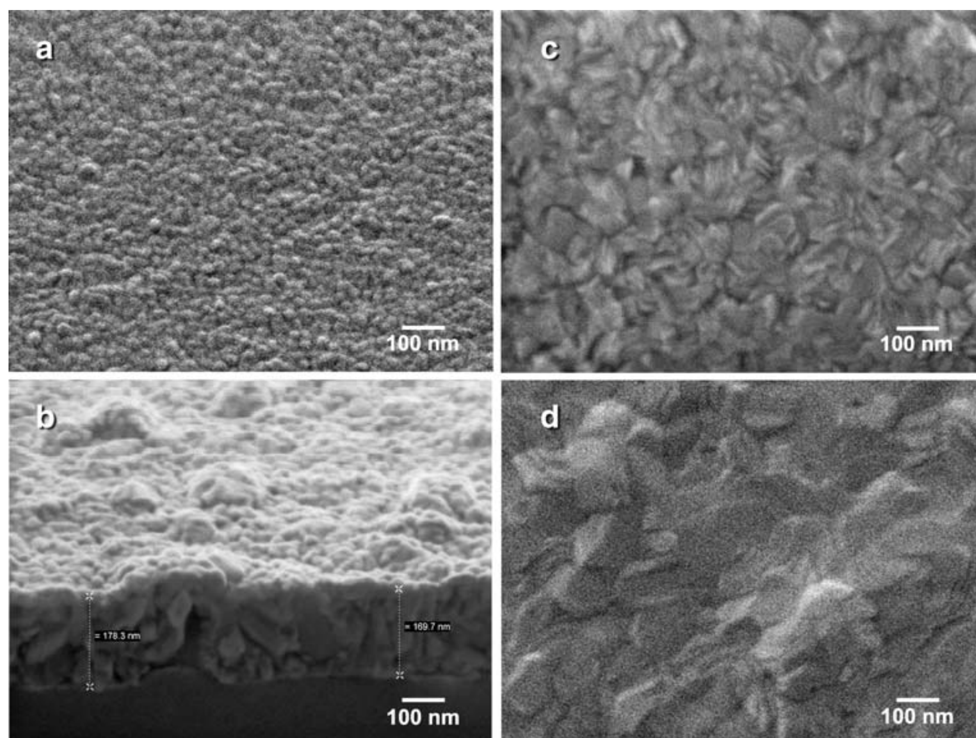

Fig. 1 Scanning electron microscopy images of **a** a 150-nm-thick Ti film covered by a 10-nm-thick Pd layer, before annealing (surface view), **b** a 100-nm-thick TiD_y film covered by a 10-nm-thick Pd layer, before annealing (cross-section view), **c** sample in **a** after annealing (surface view, normal direction) and **d** sample in **b** after annealing under similar conditions as in **c** (surface view, normal direction)

respectively [15–17]. The XPS spectra were recorded using an Al anode (beam diameter 100 µm, power 25 W). XPS sputter depth profiling was done using a 2-keV argon ion beam, a sputter area of 3×3 mm and a sputter rate of 4.7 nm/min, calibrated on a 100-nm-thick SiO_2 layer thermally grown on a Si substrate. Elemental quantification was done with standard single element sensitivity factors using CasaXPS software. The photoelectron peaks considered were O 1*s*, Pd 3*d* and Ti 2*p*.

Results and discussion

SEM analysis of film surface morphology

Figure 1 shows SEM images of the Ti/Pd and TiD_y/Pd film surfaces (Fig. 1a,b, respectively) and the corresponding film surfaces viewed after a similar annealing procedure (Fig. 1c,d, respectively).

A homogenous granular structure with a grain size of 20–40 nm can be observed on the Ti film covered by a 10–12-nm-thick Pd layer (Fig. 1a). However, in the cross-sectional SEM image of the Pd/TiD_y layer (Fig. 1b) one can observe a rough surface, superimposed on a fine-grained structure, which is determined by the grain distribution within the bulk of the TiD_y film.

A distinct change in the morphology of both film surfaces was observed after annealing. The Ti/Pd films exhibit a fibrous grain transition structure (Fig. 1c), whereas the TiD_y/Pd film, in which the annealing is accompanied by decomposition of the TiD_y phase, reveals a distinct surface structure with polygonal clusters with sizes between approximately 40 and 200 nm (Fig. 1d). This is most likely the result of the aggregation of smaller grains. The appearance of a specific fibrous structure of the annealed Ti/Pd film can be associated with a transition structure consisting of densely packed fibrous grains, which was specified in a structure zone model (SZM) developed by Thornton [18]. This model describes the film morphology as a function of the ratio of the specific substrate temperature (T_s) and melting temperature (T_m). According to this model the fibrous structure is suggested to occur at a T_s/T_m ratio of 0.1–0.5. Considering our experimental conditions during the Ti/Pd film annealing (T_s=800 K, T_m(Pd)=1828 K [19] and T_m(Ti)=1941 K [19]), we can estimate this ratio to be about 0.4 for both metals, which is consistent with the SZM prediction.

XRD analysis

Figure 2 shows XRD diffractograms taken from Ti/Pd and TiD_y/Pd films before and after annealing, all experimental procedures being performed under similar experimental conditions. By analyzing the XRD patterns, we characterized the bulk film morphology from a rough estimation of the grain size as determined from the full width at half maximum (FWHM) of XRD peaks using the Scherrer formula [20]:

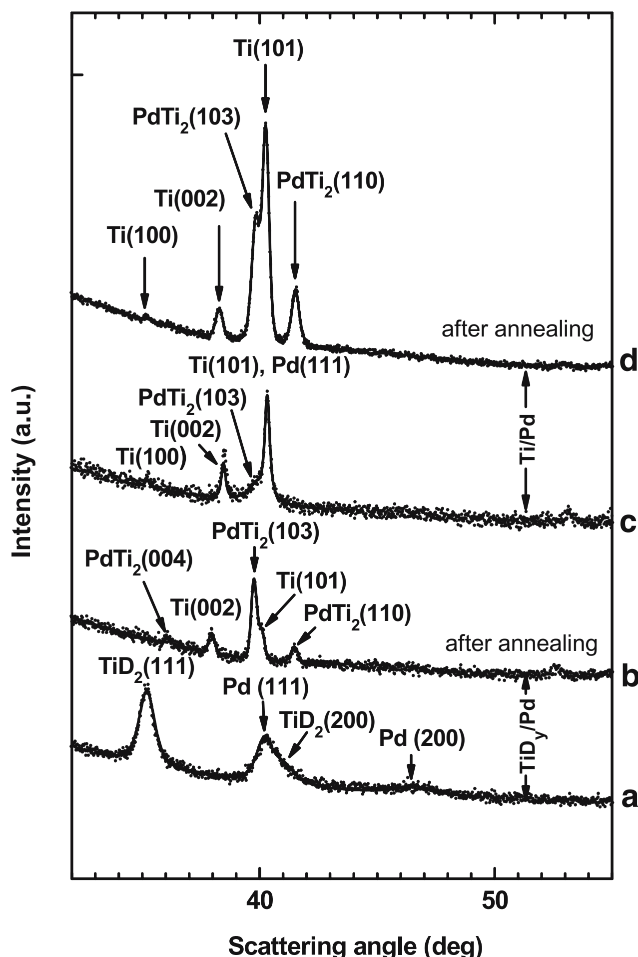

Fig. 2 X-ray diffraction (XRD) patterns of a 100-nm-thick TiD_y film covered by a 10-nm-thick Pd layer before (*a*) and after (*b*) annealing, The corresponding XRD patterns for a 150-nm-thick Ti film covered by a 10-nm-thick Pd layer, taken before and after annealing under similar conditions as in spectrum *b*, are shown in spectra *c* and *d*, respectively

$$L = K\lambda/(\beta\cos\theta) \tag{1}$$

where L is the mean crystallite size, K is a shape constant (approximately 0.9), λ is the wavelength of the X-ray radiation, β is the FWHM of the diffraction peak and θ is the Bragg angle of diffraction. Table 1 shows the results of this analysis.

It can be seen from Fig. 2 that the recorded spectra do not indicate any detectable titanium oxide phase, confirming the good protection properties of the Pd layer against destructive air interaction [9, 10]. The XRD pattern for the TiD_y/Pd film (spectrum a) exhibits a face-centered cubic

Table 1 Mean crystallite size evaluated from the X-ray diffraction patterns of a 150-nm-thick Ti film and a 100-nm-thick TiD_y film, both covered by a 10-nm-thick Pd layer, before and after annealing (see Fig. 2) using the Scherrer formula [20]

Material	Mean crystallite size (nm)
Ti/Pd film (prior to annealing)	40.1±0.3 (Ti, Pd)
	7.0±0.3 ($PdTi_2$)
Ti/Pd film (after annealing)	24.2±1.0 (Ti)
	20.8±0.7 ($PdTi_2$)
TiD_y/Pd film (prior to annealing)	12.1±0.3 (TiD_2)
	10.8±0.3 (Pd)
TiD_y/Pd film (after annealing)	32.0±0.1 (Ti)
	23.7±0.7 ($PdTi_2$)

(fcc) CaF_2-like structure of the TiD_y(δ-phase TiD_2) [21] with a dominant (111) orientation and a distinct fcc Pd phase [21]. Upon annealing, the TiD_y/Pd film undergoes a structural transformation (spectrum b). A new tetragonal bimetallic $PdTi_2$ phase [21] appears in addition to the Ti hexagonal close packed (hcp) phase [21]. The same $PdTi_2$ phase grows within the Ti/Pd film as a result of annealing (spectrum d). The annealing process is accompanied by significant changes in the size of the crystallites forming the crystalline phase in both Ti/Pd and TiD_y/Pd films. The mean size of the $PdTi_2$ and Ti crystallites was found to be relatively larger in the annealed TiD_y/Pd film than in the corresponding Ti/Pd film (Table 1). This tendency was also observed by SEM (Fig. 1), reflecting the surface morphology variations of both films due to annealing.

The question arises of what the relative contribution of $PdTi_2$ is in the crystalline phase of the annealed TiD_y/Pd film compared with the corresponding Ti/Pd film. To consider this point more quantitatively, we compared the XRD peak areas evaluated for the Ti and $PdTi_2$ phases in both annealed films. The relative ratio of the XRD peak areas attributed to the $PdTi_2$ and Ti phases was calculated to be 0.7 and 2.0 for the annealed Ti/Pd (Fig. 2, spectrum d) and TiD_y/Pd (Fig. 2, spectrum b) films, respectively. This indicates that the relative contribution of $PdTi_2$ in the crystalline phase of the annealed TiD_y/Pd film is significantly higher than in the corresponding Ti/Pd film.

The XRD pattern of the annealed TiD_y/Pd film (Fig. 2, spectrum b) reveals the most relevant peaks, which can be attributed to the tetragonal $PdTi_2$ phase [(103) and (110)], as well as a low-intensity (004) peak. However, in the annealed Ti/Pd film (Fig. 2, spectrum d) no $PdTi_2$ (004) peak was detected. The absence of this diffraction peak is likely to be due to a partial distortion of the $PdTi_2$ phase, which is formed in coexistence with the Ti hcp phase, and indicates that the path of annealing-induced formation of the $PdTi_2$ phase in the Ti/Pd film is different from that in the TiD_y/Pd film.

It is interesting to note that a weak $PdTi_2$(103) peak is already observed in the XRD spectrum of the Ti/Pd film before annealing (Fig. 2, spectrum c); this spectrum can be characterized by a relatively small Pd(111) peak and absence of the Pd(200) peak. The result supports the idea that the fcc Pd structure becomes significantly distorted already during low-temperature evaporation of Pd on the Ti film because of $PdTi_2$ phase growth initiation. The crystalline Pd fraction of the bimetallic film is reduced by interaction with Ti owing to the formation of an amorphous bimetallic phase within the Pd–Ti interface region. A similar phenomenon was observed by Tadayyon et al. [22] in sputter-deposited Pd/Ti multilayer films. The authors showed that an amorphous phase is formed in the interface region even for deposition at room temperature, and that the amorphization also proceeds during postdeposition annealing at 573–623 K. According to their model [22], the thermodynamic driving force for the reaction between crystalline Pd and Ti layers to form the amorphous alloy is the result of a large negative heat of mixing of both metals [22]. In our case the annealing of the Ti/Pd film was performed at higher temperature (800 K), in which the amorphization of the Ti and Pd crystalline phases within the Ti–Pd interface, observed prior to annealing (Fig. 2, spectrum c), is followed by a high-temperature-induced recrystallization of the Ti phase and intensive growth of the new $PdTi_2$ crystalline phase. The recrystallization process leads to an increase of all XRD peaks of the annealed Ti/Pd film (Fig. 2, spectrum d). The analysis of the XRD patterns recorded for the Ti/Pd films prepared prior to annealing (Fig. 2, spectrum c) and processing by annealing (Fig. 2, spectrum d) reflects a significant growth of the $PdTi_2$ crystallites after annealing (compare the mean crystallite size of $PdTi_2$ in the Ti/Pd film prior to and after annealing, presented in Table 1).

XS-TEM analysis

Figure 3 shows low-magnification TEM cross-sectional images of TiD_y/Pd (Fig. 3a) and Ti/Pd (Fig. 3b) films, both annealed under the same experimental conditions. The images reveal a complex bulk structure containing distinct, randomly distributed crystallites in addition to disordered regions, which can be ascribed to the formation of an amorphous phase in both films. In a previous paper [10], we showed similar amorphous structures appearing within the interface region of the Pd/Ti bilayer films evaporated at room temperature.

In order to obtain information on the microstructure of both annealed films SAD analyses were carried out on the cross-section planes. Figure 3c and d shows a quarter-section representation of the SAD pattern from the annealed TiD_y/Pd and Ti/Pd films, respectively. All SAD recordings

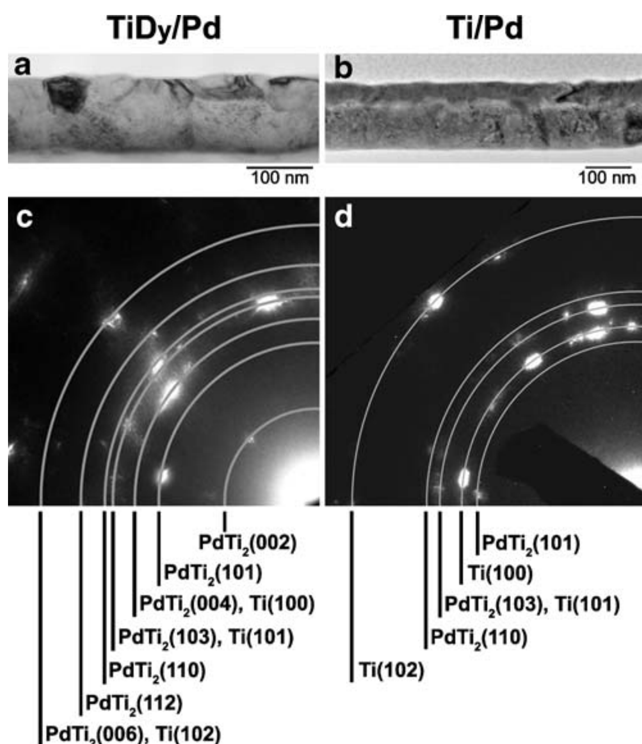

Fig. 3 Low-magnification transmission electron microscopy (TEM) cross-sectional bright-field images of the annealed TiD_y/Pd (**a**) and Ti/Pd (**b**) films. The selected area diffraction patterns recorded on the annealed TiD_y/Pd and Ti/Pd areas are shown in **c** and **d**, respectively, in a quarter-section representation, together with the assignment of the most relevant low-index Miller planes of the diffraction spots

show the diffraction spots to lie on artificial concentric circles (semitransparent gray circle sections drawn on SAD spot patterns). From a direct measurement of the radius between the central spot and the relevant diffraction spots lying on these artificial concentric circles, the Miller index planes can be determined. This allows the crystallographic planes belonging to Ti hcp [21] and tetragonal $PdTi_2$ [21] structures to be identified. For an assignment of the most relevant low-index Miller planes, see Fig. 3c and d.

EF-TEM and EDX analysis

EF-TEM analysis on the cross-section planes was carried out in order to reveal the relative distribution of Ti and Pd atoms as a result of annealing the Ti/Pd and TiD_y/Pd films. In Fig. 4 the results of such analysis, performed on both films, are presented. In the left column a high-magnification XS-TEM image of the Ti/Pd film is shown together with the associated EF-TEM elemental mapping images of Pd ($M_{4,5}$ edge) and Ti ($L_{2,3}$ edge). The elemental distribution is marked in white color. In the right column the corresponding images for the TiD_y/Pd film are compared.

EF-TEM analysis reveals that an extensive intermixing process between the Ti and Pd layers forming the bilayer films occurs as a result of the annealing process. The range of major Pd atom penetration into the Ti and TiD_y layers, revealed by the EF-TEM mapping images (Fig. 4), is on the order of 25–40 nm for both annealed films, which is much larger than the thickness of the deposited Pd layer (approximately 10 nm) covering both the Ti and the TiD_y films prior to annealing [10]. Such a significant spread of the Pd–Ti intermetallic phase within bilayer films can be explained in terms of high-temperature-induced interdiffusion processing [23]. To consider this point we can estimate the length of the diffusion zone (L_{diff}) for Ti and Pd within the Pd–Ti interface, which is available from the annealing time (τ_{diff}), using the simple relation $\tau_{diff}=(L_{diff})^2/D_{diff}$,

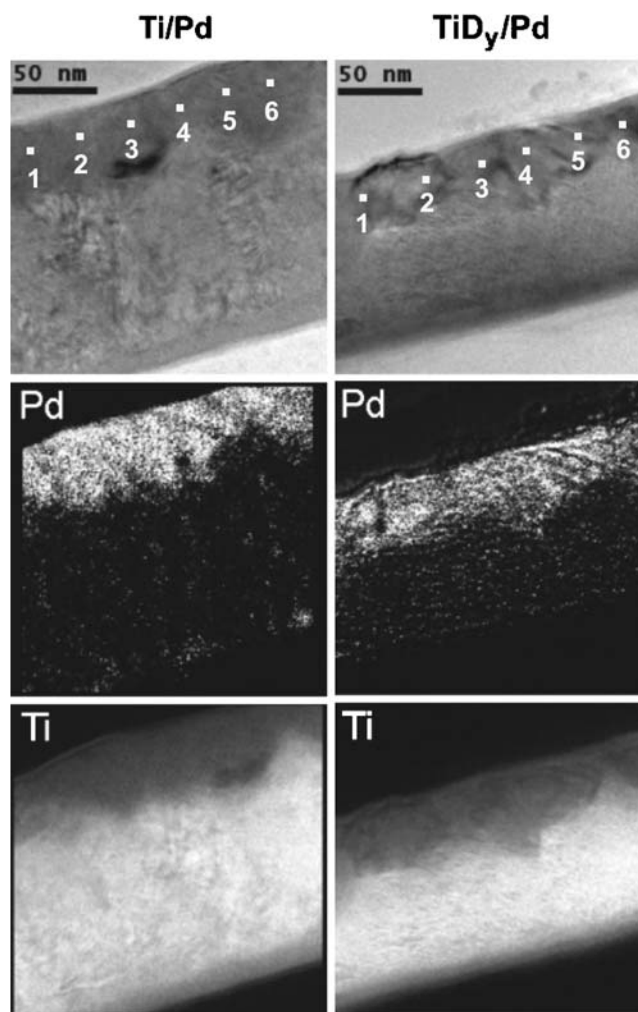

Fig. 4 Energy-filtered TEM analysis of the Ti/Pd (*left column*) and TiD_y/Pd (*right column*) films after a similar annealing procedure (see text for details). The bright-field cross-sectional TEM images of both films are presented at the top of each column. The spots marked *1–6* show the areas analyzed by energy-dispersive X-ray spectrometry using a focused primary electron beam of 3.5-nm diameter. Below the cross-sectional TEM images are shown the associated elemental mapping images of Pd ($M_{4,5}$ edge) and Ti ($L_{2,3}$ edge). The elemental distribution is marked in *white*

where D_{diff} is a diffusion coefficient determined for each metal at the annealing temperature. Taking the literature value of D_{diff} for Pd and Ti diffusion in Pd/Ti bilayer films to be 1.2×10^{-19} and 1.7×10^{-19} m^2 s^{-1}, respectively [23], and τ_{diff}=2 h, we can estimate L_{diff} to be 29 and 35 nm, respectively, for the Pd and Ti diffusion zone. These values are in agreement with our EF-TEM results.

Close inspection of the EF-TEM images in Fig. 4 shows also that Ti atoms seem to penetrate more extensively into the Pd-rich layer of the annealed TiD_y/Pd film than into the Ti/Pd film. Compare, e.g., the intensity of the white dots in the two Pd mappings; the higher the intensity, the higher the relative concentration of Pd in this layer, and consequently the lower the concentration of Ti. The Pd-rich layer of the TiD_y/Pd film shows darker regions in the Pd map than that in the Ti/Pd film. The intensity of the Ti signal in the corresponding Ti mapping of the TiD_y/Pd film is, on the other hand, on average slightly higher than in the Ti/Pd film. This result suggests that high-temperature-induced decomposition of deuteride modifies the interdiffusion process, promoting more Ti diffusion into the Pd-rich top-film region and making it more likely that a $PdTi_2$ phase is formed. In order to verify this observation EDX analysis was carried out within the top-layer film area of both films. On six different spots of each film, lying at a similar distance from the top of the film in cross section, a local EDX analysis was carried out using a focused primary electron beam of 3.5-nm diameter. The measured spots in Fig. 4 are marked with numbers 1–6. The EDX analysis results for all spots are summarized in Table 2. EDX quantification using the thin-film approximation (standardless quantification routine according to the Cliff–Lorimer approximation without absorbance), performed as an average for six measured spots (see the results in Table 2), reveals the Ti-to-Pd ratio to be 1.3±0.1 for the Ti/Pd film. A strong variation in the Ti-to-Pd ratio was, however, found within the top layer of the annealed TiD_y/Pd film. The Ti-to-Pd ratios were estimated to be in the range 0.3–11.5 (Table 2). Such strongly varying ratios can be the result of significant TiD_y film surface roughness, leading to TiD_y–Pd interface irregularities, subsequently affecting the area within the Ti diffusion zone in the Pd top layer. To obtain an average value of the Ti-to-Pd ratio in the annealed TiD_y/Pd film we measured the EDX signal using a defocused circular-shaped electron beam until the entire film from top to bottom in cross section was included in the analysis. The total Pd intensity EDX signal was then compared with the Ti intensity measured locally along the Pd–Ti intermetallic zone layer (see the EF-TEM mapping images in Fig. 4). The average Ti-to-Pd ratio evaluated in this way was 2.3. The results of these calculations confirm more extensive Ti atom penetration within the Pd top layer of the TiD_y/Pd film than in the Ti/Pd film. It is also relevant to point out that the roughly evaluated Ti-to-Pd ratio from EDX is in reasonable agreement with the stoichiometry of the $PdTi_2$ compound.

Table 2 Energy-dispersive X-ray spectrometry analysis results for the selected areas of the annealed Ti/Pd and TiD_y/Pd films

Sample	Area	Ti-to-Pd ratio (atom %)
Ti/Pd film (after annealing)	1	1.33
	2	1.44
	3	1.33
	4	1.27
	5	1.38
	6	1.22
TiD_y/Pd film (after annealing)	1	0.82
	2	1.33
	3	0.89
	4	1.63
	5	0.33
	6	11.50

The measured areas are marked in Fig. 4 with numbers (1–6) for each film. The analysis was carried out using a focused primary electron beam of 3.5-nm diameter

XPS analysis

The chemical nature of the components formed within the surface region of the annealed Ti/Pd and TiD_y/Pd films was investigated by means of XPS. Figure 5 shows a set of Pd 3*d* (panel a), Ti 2*p* (panel b), O 1*s* (panel c) and valence band (panel d) XPS spectra presented for both films. All these spectra were recorded after the films had been etched with argon ions for 2 min to remove the air contaminants. As can be seen, the XPS spectra do not reveal any chemical differences in the surface and subsurface regions between the two systems.

In Fig. 6, Pd 3*d* (panel a) and Ti 2*p* (panel b) spectra of the annealed TiD_y/Pd film recorded before and after argon ion etching are compared with the corresponding XPS spectra collected on separate pure Pd and Ti films. In this way we can better investigate the shift in the BE of Ti and Pd peaks as a result of annealing the TiD_y/Pd film, so that the chemical nature of the intermetallic compounds formed within both annealed bimetallic films can be identified more accurately.

The Pd 3*d* XPS spectrum (Fig. 6, panel a) of the “as received” annealed TiD_y/Pd film (spectrum 1) is characterized by a doublet in the Pd 3*d* spectrum (Pd $3d_{5/2}$ peaks positioned at BE=335.7 and 336.5 eV and corresponding Pd $3d_{3/2}$ peaks at BE=340.9 and 341.7 eV, respectively). This spectrum is accompanied by the O 1*s* XPS spectrum at BE=530.0 eV (spectrum 1 in Fig. 6, panel c) and the Ti 2*p* XPS spectrum formed by a Ti $2p_{3/2}$ peak at BE=459 eV and

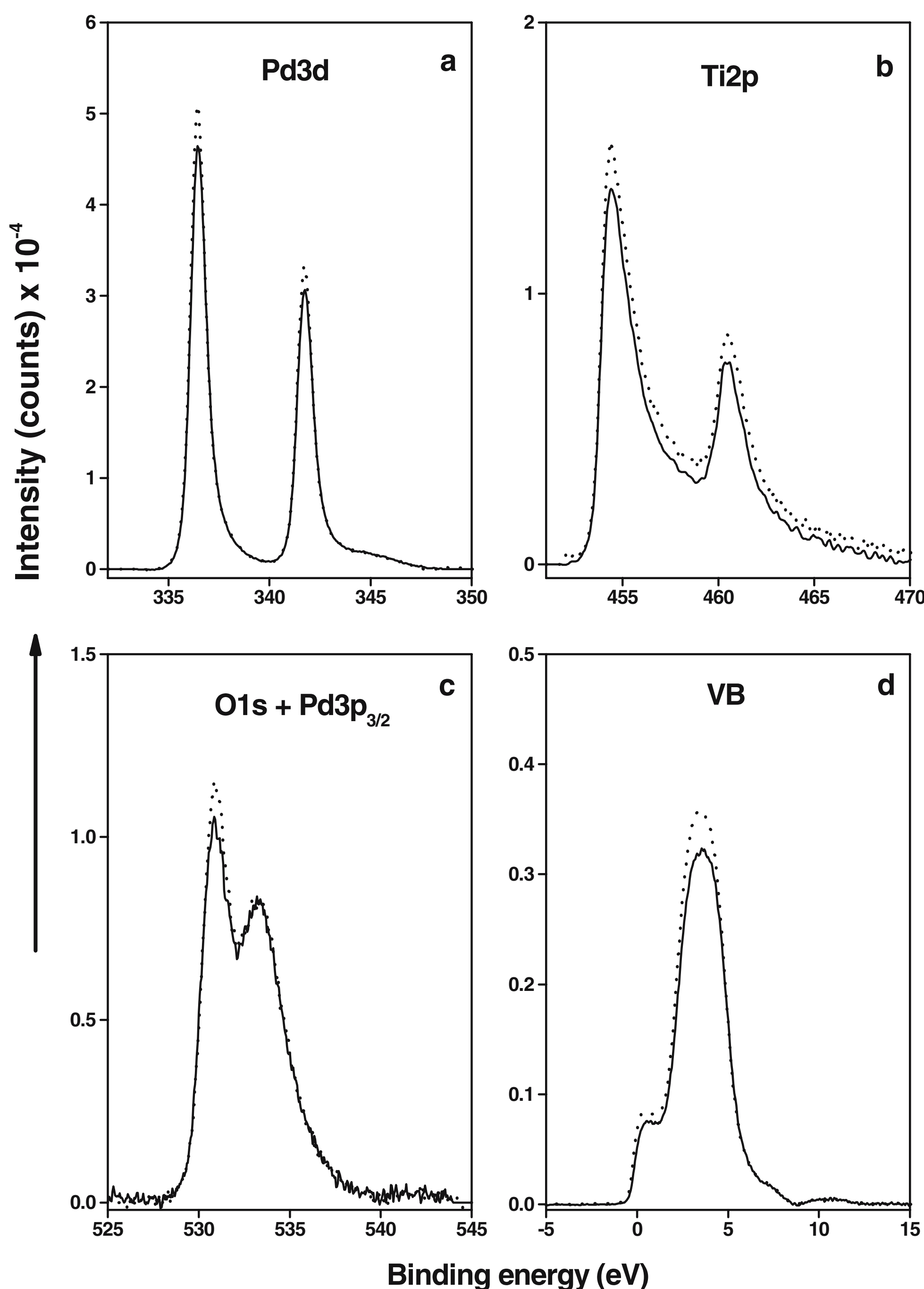

Fig. 5 Pd 3*d* (**a**), Ti 2*p* (**b**), O 1*s* + Pd $3p_{3/2}$ (**c**) and valence band (*VB*) (**d**) X-ray photoelectron spectroscopy (XPS) spectra of the TiD_y/Pd (*dotted lines*) and Ti/Pd (*solid lines*) films, recorded after identical annealing processes. Both samples were argon ion etched for 2 min (sputter rate of 4.7 nm/min)

a Ti $2p_{1/2}$ peak at BE=464.7 eV (spectrum 1 in Fig. 6, panel b), which is indicative of heavy contamination with TiO_2 [24] and PdO [24]. After a short argon ion sputter cleaning cycle, only a single Pd $3d_{5/2}$ peak emerges, increasing at BE=336.5 eV (spectrum 2). Therefore, we can ascribe the Pd $3d_{5/2}$ peak at BE=335.7 eV to surface palladium oxide. When the Pd $3d_{5/2}$ peak at BE=336.5 eV (spectrum 2 in Fig. 6, panel a) is compared with the corresponding peak from the pure Pd film (spectrum 3 in Fig. 6, panel a), the observed 1.4-eV BE shift relative to pure Pd shows good agreement with the corresponding BE shift of 1.37 eV, reported by Bzowski and Sham [25] for $PdTi_2$. These authors determined in addition the BE shift of the Ti $2p_{3/2}$ peak for $PdTi_2$, which was found to be 0.33 eV relative to pure Ti. This value is very close to the BE shift (0.4 eV) derived from our spectra (compare spectra 2 and 3 in Fig. 6, panel b). The characteristic features of the valence band spectra recorded on both annealed films (see valence

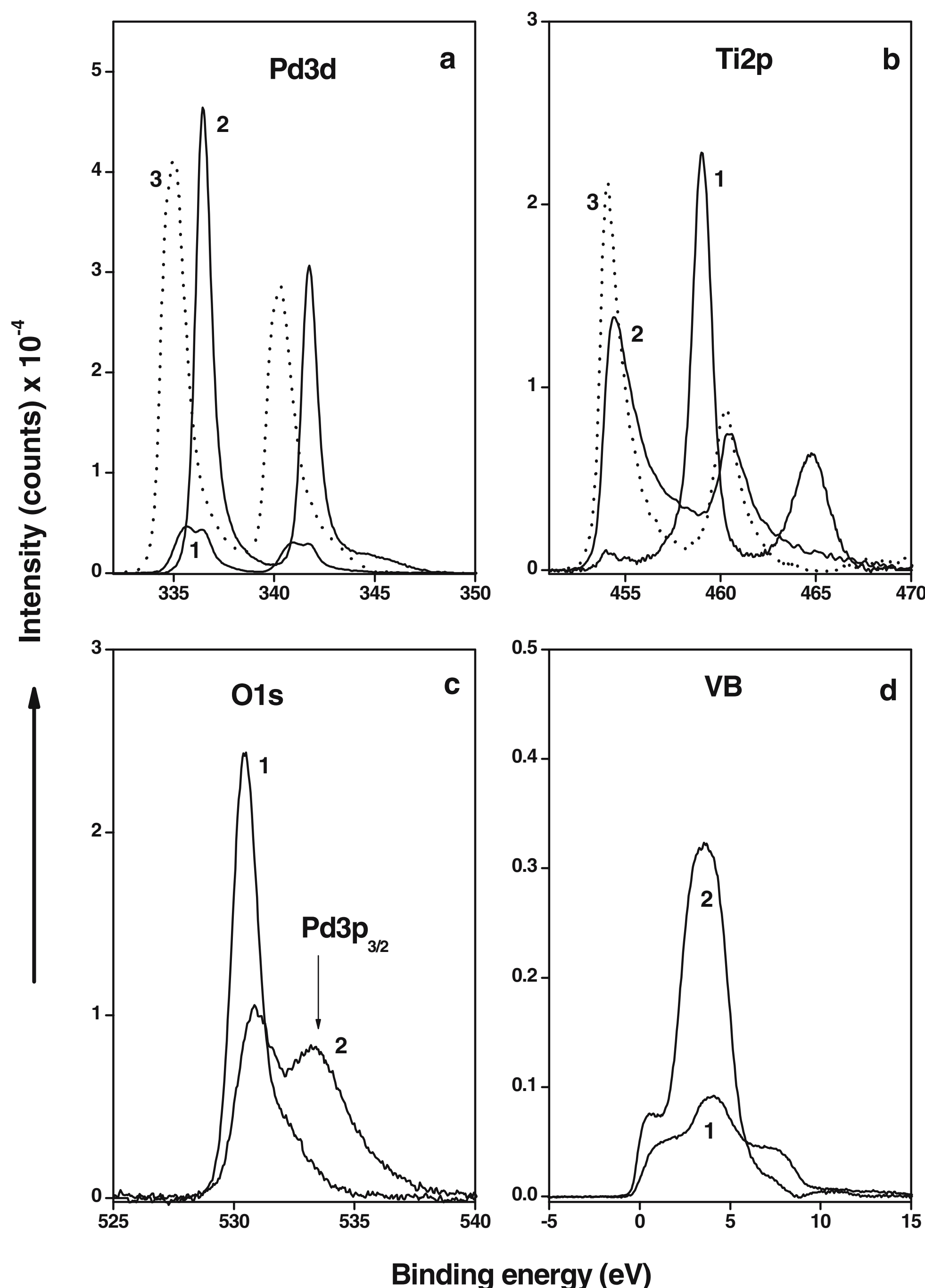

Fig. 6 Pd 3*d* (**a**), Ti 2*p* (**b**), O 1*s* + P*d* $3p_{3/2}$ (**c**) and VB (**d**) XPS spectra collected on the annealed TiD_y/Pd film. The "as received" spectra (*lines 1*) are compared with the spectra taken on the same film after 2 min of argon ion sputter cleaning (*lines 2*) and with the spectra recorded on separate pure Pd and Ti films (*dotted lines 3*)

band peaks at BE=0.5 and 3.5 eV in Fig. 5, panel d and Fig. 6, panel d) are also in accordance with the data presented in [25]. $PdTi_2$ therefore seems to be the most likely intermetallic compound appearing within the TiD_y/Pd and Ti/Pd films due to the annealing process. Our XPS results further corroborate the idea of a $PdTi_2$ phase appearance during heating-induced structural transformation of both films as derived from XRD (see "XRD analysis) and TEM/EDX (see "EF-TEM and EDX analysis").

XPS depth-profiling analysis

The TiD_y/Pd and Ti/Pd films were depth-profiled using XPS to elucidate the Pd and Ti distribution within both films after the annealing procedure. Because both annealed films contain the same chemical compounds, and were analyzed under the same experimental conditions, we assume that all sputter-profiling-induced effects, like instrument-related effects, surface effects and bulk-atomic

mixing [26], are similar for both films. Therefore, in a direct comparison of the elemental depth profiles for both films these sputter-profiling-induced artifacts are cancelled out, thus disclosing only the difference in the Pd and Ti distribution in both films caused by the annealing process.

Figure 7 shows the XPS depth profiles of the annealed Ti/Pd (panel a) and TiD_y/Pd (panel b) films. The depth distribution of O, Pd and Ti evaluated from the O 1*s*, Pd 3*d* and Ti 2*p* XPS peaks, respectively, is shown as a function of sputter depth, which was roughly calculated taking a sputter rate of 4.7 nm/min, which was calibrated against a well-known reference material (SiO_2/Si). We assumed this sputter rate to be correct because the Pd depth distribution, as evaluated from the Pd 3*d* XPS depth profile (Fig. 7, panels a and b), appeared to be equal to the thickness of the Pd zone revealed by the EF-TEM elemental mapping images (Fig. 4).

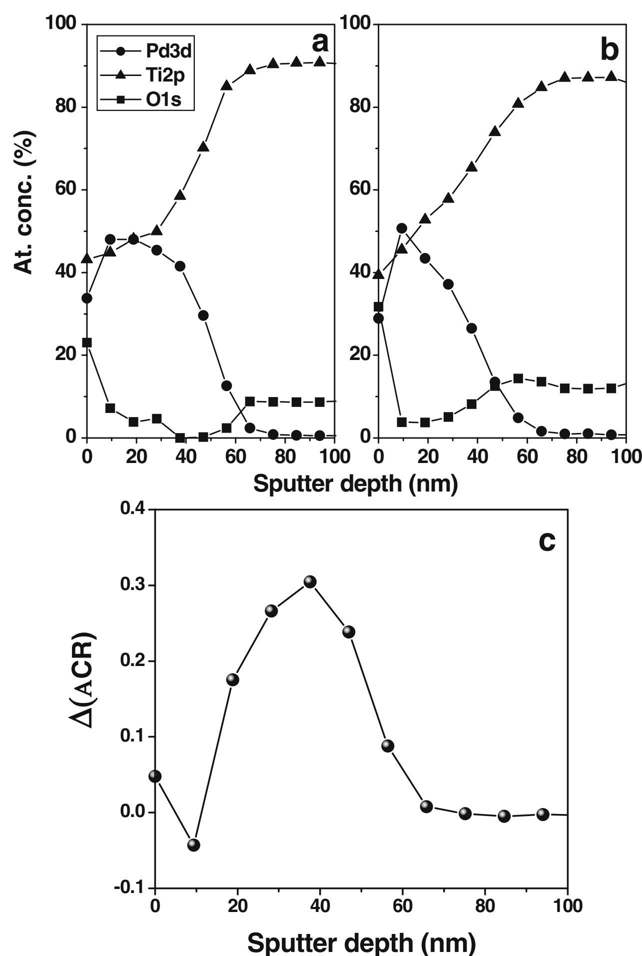

Fig. 7 XPS sputter depth profiles of the Ti/Pd (**a**) and TiD_y/Pd (**b**) films. The atomic concentration depth distribution of O, Pd and Ti evaluated from the O 1*s*, Pd 3*d* and Ti 2*p* XPS peaks are shown as a function of sputter time (sputter rate 4.7 nm/min relative to 100-nm-thick SiO_2). In *panel* ***c*** the difference of the Pd-to-Ti atomic concentration ratio [*Δ(ACR)*], determined from the XPS profiles of both compared films is shown as a function of sputter time. For a description, see the text

The Pd top layer is supposed to protect both Ti and TiD_y films against interaction with oxygen from the air. However, a small degree of oxygen is still detected within the bulk of both films. These small amounts of oxygen are probably due to the release of oxygen from the tungsten heater during the Pd film after evaporation, since this heater cannot be completely out-gassed before Pd film deposition starts owing to the relatively low temperature of Pd evaporation [27].

The most relevant elemental distribution differences can be observed during depth profiling of the top region of both films. We can see that the Ti atoms penetrate the top region of the TiD_y/Pd film much more extensively (compare the Ti 2*p* profiles of the Ti/Pd and TiD_y/Pd films in Fig. 7, panels a and b, respectively). To show this more clearly, we compared the relative Pd 3*d* to Ti 2*p* atomic concentration ratios (ACR) evaluated from the XPS depth profiles of both films. The difference of these values, expressed as Δ(ACR)=ACR(Ti/Pd film) - ACR(TiD_y/Pd film), is shown in Fig. 7, panel c as a function of sputter depth. The Δ(ACR) profile shows a significantly higher Pd-to-Ti ratio within the top region of the Ti/Pd film than in the TiD_y/Pd annealed film. Or, alternatively formulated, the relative concentration of Ti atoms within the top of the TiD_y/Pd film is higher than in the Ti/Pd film. This result is consistent with the EFTEM and EDX data (see "EF-TEM and EDX analysis").

Summary and conclusions

It was found that annealing of TiD_y/Pd and Ti/Pd films, performed under identical conditions, leads to different film structure transformations. The Ti/Pd film surface morphology, as revealed by SEM, is characterized by a fibrous grain transition structure, whereas the TiD_y/Pd film, in which decomposition of the TiD_y phase occurs during annealing, reveals a distinct surface structure with polygonal clusters. Upon annealing, EF-TEM elemental mapping and local EDX analyses along the bilayer films in cross section, revealed an extensive intermixing of Ti and Pd. XRD and XPS provided evidence for the formation of a new $PdTi_2$ bimetallic phase within the top region of both annealed films. However, the annealing-induced decomposition of deuteride modifies the intermixing process, promoting more Ti diffusion into the Pd-rich top layer of a TiD_y film, so $PdTi_2$ phase formation is more likely to occur in TiD_y systems. The combination of EF-TEM, EDX and XPS provided a coherent picture of this phenomenon. And the results presented indicate that a thin Ti/Pd film may be useful in its practical utilization as hydrogen (deuterium) storage material.

References

1. Westlake DG, Satterthwaite CB, Weaver JH (1978) Phys Today 31:32–39
2. Hirooka Y (1984) J Vac Sci Technol A 2:16–21
3. Kirchheim R, Fromm E, Wicke E (eds) (1989) Metal-hydrogen systems: fundamentals and applications. Proceedings of the first international symposium combining “hydrogen in metals” and “metal hydrides” Stuttgart, 1988. Oldenburg, Munich
4. Wedler G, Strothenk H (1966) Z Phys Chem Neue Folge 48:86–101
5. Malinowski ME (1979) J Vac Sci Technol 16:962–963
6. Checchetto R, Gratton LM, Miotello A, Tomasi A, Scardi P (1988) Phys Rev B 58:4130–4137
7. Lisowski W, van den Berg AHJ, Smithers M (1998) Surf Interface Anal 26:213–219
8. Lisowski W, van den Berg AHJ, Leonard D, Mathieu HJ (2000) Surf Interface Anal 29:292–297
9. Heller EMB, Suyver JF, Vredenberg AM, Boerma DO (1999) Appl Surf Sci 150:227–234
10. Lisowski W, Keim EG, van den Berg AHJ, Smithers MA (2006) Anal Bioanal Chem 385:700–707
11. Lisowski W (1999) Vacuum 54:13–18
12. Duś R, Lisowski W, Nowicka E, Wolfram Z (1995) Surf Sci 322:285–292
13. Lisowski W, Keim EG, Smithers MA (2003) J Vac Sci Technol A 21:545–552
14. Lisowski W, Keim EG, Smithers M (2002) Appl Surf Sci 189: 148–156
15. Anthony MT (1983) In: Briggs D, Seah MP (eds) Practical surface analysis by Auger and X-ray photoelectron spectroscopy. Wiley, Chichester, p 431
16. Ikeo N, Jijima Y, Niimura N, Sigematsu M, Tazawa T, Matsumoto S, Kojima K, Nagasawa Y (1991) Handbook of X-ray photoelectron spectroscopy. JEOL, Peabody
17. Seah MP (1999) Appl Surf Sci 144–145:161–167
18. Thornton JA (1977) Ann Rev Mater Sci 7:239–260
19. Winter M (1993–2007) WebElements periodic table. http://www.webelements.com
20. Patterson AL (1939) Phys Rev 56:978–982
21. Joint Committee on Powder Diffraction Standards, ICDD (1999) Powder diffraction file. Pd: card 46–1043, Ti: card 44–1294, $TiH_{1.971}$: card 07–0370, $PdTi_2$: card 18–0957
22. Tadayyon SM, Fujimoto Y, Tanaka K, Doi M, Matsui M (1994) Jpn J Appl Phys 33:4697–4702
23. Tadayyon SM, Yoshinari O, Tanaka K (1993) Jpn J Appl Phys 32:3928–3932
24. Wagner CD, Naumkin AV, Kraut-Vass A, Allison JW, Powell CJ, Rumble JR Jr (2003) NIST Standard Reference Database 20, version 3.4. http://srdata.nist.gov/xps/
25. Bzowski A, Sham TK (1993) Phys Rev B 48:7836–7840
26. Andersen HH (1979) Appl Phys 18:131–140
27. Honig RE (1962) RCA Rev 23:567–586